RSC Advances

ROYAL SOCIETY
OF CHEMISTRY

www.rsc.org/advances

RSC Advances

RSC**Publishing**

COMMUNICATION

Growth Mechanism of Curved Mg-Al-CO₃ Layered Double Hydroxide Nanostructures in a One-pot Assembling Procedure under Ambient Pressure

Xinxin Zhao, Chenggang Zhou*, Bo Han, Zhuan Ji, Liang Wang and Jinping Wu*

We discovered that the adding amount of peroxide is a governing factor that lead to curved or amorphous morphologies of Mg-Al-LDH products in a reflux system under ambient pressure. A concerted growth mechanism was proposed to elucidate the formation of the unconventional nano-features of the products.

Introduction

Layered double hydroxides (LDHs), with a general formula of $[M^{2+}_{1-x}M^{3+}_x(OH)_2]A^{n-}_{x/n} \cdot mH_2O$, are composed by layered planar sheets of M^{2+}/M^{3+} hydroxides and the interlayer A^{n-} anions[1-8]. By assembling functional agents to the delaminated LDHs[9-12], a broad variety of applications may be developed involving polymer/LDH nanocomposite[13-21], functional thin films[22-25], catalysts[26, 27], electrode materials[28-33], photo-functional materials[34, 35] and bioinorganic hybrid materials[36]. Appropriate and simple delamination method is consequently required before functionalization. Typically, there are two strategies for delaminating LDH compounds as named by "bottom-up" and "top-down"[1]. For the bottom up synthesis, LDH products were typically prepared via the microemulsion mediated hydrothermal synthesis. The size of the particles can be controlled both in diameter and thickness by tuning the water to surfactant ratio in different reverse microemulsion systems[37-44]. In parallel, large amount of efforts have been focused on the delamination of LDHs by the top down synthesis in polarized solvents such as butanol[45-47], acrylates[10], formamide[48-52] and N,N-Dimethylformamide/ethanol mixture[53-55], nonpolarized solvents such as CCl₄[56-58], and other type of solvents[59, 60]. i. e. Adachi-Pagano et al[45] reported the complete delamination of the Zn-Al-LDH using sodium dodecyl sulfate (SDS) as an anionic surfactant and butanol as the dispersant. Ma et al[61] exfoliated Co-Fe-LDHs into nanosheets in formamide by an ultrasonic treatment through hexamethylenetetramine (HMT) hydrolysis. Wu et al[62] reported the direct delamination of Mg-Al-NO₃ in formamide using ultrasonic treatment at room temperature. The obtained delaminated LDH products in these reports generally exhibit as unilamellar sheets. However, for applications such as catalysis, sensing and electrochemical

energy storage devices, designing appropriate client-substrate interaction for the functionalized LDH products should become more important for the desired physicochemical properties[63-65]. To this end, unconventional curved LDHs could provide higher surface area, metal dispersion, morphological structure, reduction properties, porosity[66], which would of course increase the accessibility to both the internal galleries and the outer surface comparing with typical plane LDHs[67-72].

Several reports have synthesized nonconventional LDH morphologies and found they exhibit interesting sensing[73], catalytic[74], photocatalytic[75], and supercapacitive[76-79] performances. i. e. Adachi-Pagano et al[80] reported the sand-rose morphology of Mg-Al-LDHs using urea hydrolysis method in a mixture solvent of water and ethylene glycol (EG). The size distribution of the mono-dispersed particles are determined by the water/EG ratio, urea concentration and the Mg/Al ratio. The preferential adsorption of EG on the (00l) planes of Mg-Al-LDH prevents the growth at the direction perpendicular to the layers, leading to the inhibition of particle ripening and resulting in the as-obtained sand-rose morphologies. The same phenomenon was observed by Wei et al[81] when synthesizing Li-Al-LDHs using urea method in a water/ethanol mixture solvent, where the Ostwald ripening mechanism were employed to elucidate the formation of the polymorphic morphologies. The petal-like Li/Al LDHs show much higher specific capacitance comparing with the spiral structure and hexagonal nanosheets. Using chitosan as template, Li and coworkers[82] suggested that Ni-Al-LDH particles co-precipitated through the urea method will curve in the a direction, while the growth at both a and c directions were inhibited, resulting in curved fibre-like shapes of the products. Liu et al[65] reported the special nanoconic structures of Co-M-LDHs (M=Ni, Cu, Zn) using urea method and simultaneously intercalated dodecyl sulfate (DS) into the interlayer spaces. The LDH nanocones, owning controllable transition-metal compositions, peculiar hollow feature and large interlayer spacing, exhibit high specific capacitance and

remarkable cycling stability when serving as supercapacitor electrodes.

We mention that the polymorphic structural features of different LDH compounds generally occurred in the urea method, and the third-party agents, either organic solvent or surfactants, played an inneglecible role for forming the special spatial configuration. In fact, these third-party agents were supposed to act as inhibitor to slow down the growth at certain lattice directions or to prevent the particles from being agglomeration. Very recently, Yan et al[83] reported a one-pot approach to assemble Mg-Al-LDH nanosheets using urea method where peroxide was selected as the third-party agent. Within an autoclave environment, the prepared LDH appear as unilamellar flat nanosheets, and delamination was concluded to be implemented by the oxygen gas from the peroxide decomposition. In the present work, we implemented this one-pot process under ambient pressure within a reflux system. Interestingly, unlike in the sealed system, our procedure offered the opportunity to tune the polymorphic features of Mg-Al-LDH products by changing the peroxide concentration. In particular, with a 20 wt% addition of H_2O_2, curved or even cross-linked delaminated sheets were observed. Based on the XRD, SEM, FT-IR and TGA characterizations, we proposed a different concerted growth mechanism to explain the as-obtained curved patterns, which might be useful for understanding the synthesis of different morphologies for similar hydroxide systems.

Experimental

Preparation of the materials.

All analytical-grade chemicals utilized in our experiments were used as purchased. The Mg^{2+}, Al^{3+} precursors (appear as $Mg(NO_3)_2 \cdot 6H_2O$ and $Al(NO_3)_3 \cdot 9H_2O$, respectively) and urea were dissolved in deionized water or peroxide solution in a 500 mL round-bottom flask with a Mg^{2+}:Al^{3+}:urea molar ratio of 4:1:10 at room temperature, where the Mg^{2+} concentration was set to be 0.004 mol·L^{-1}. The following co-precipitation process was carried out within the same flask under ambient pressure with reflux. For the water solvent, we considered four bath temperature (100 ºC, 120 ºC, 150 ºC and 180 ºC) and three bath duration (3 h, 5 h and 8 h) to figure out the optimal synthesis conditions. These parameters were successively employed for the peroxide solution solvent where three different peroxide concentrations (10 wt%, 20 wt% and 30 wt%) were studied. The filtered solid products were washed by deionized water for 5 times and then dried at 60 ºC for 12 h before characterization.

Characterization techniques.

The X-ray diffraction (XRD) data of all samples were collected on a German Bruker D8-Focus powder X-ray diffractometer with Cu Kα radiation (λ=1.540598Å) at a scanning rate of 0.05 seconds per step. Thermogravimetric analysis was carried out on the TGA-DSC (STA449 F3, NETZSCH, German) instrument where the temperature range

was set to be 30-1000 °C with a heating rate of 10 °C·min^{-1} under N_2 atmosphere. Fourier-transform infrared (FT-IR) spectra were recorded with a Fisher Nicolet 6700. The scanning electron microscope (SEM) was collected on a Hitachi D8-Focus instrument at an acceleration voltage of 0.1–30 kV.
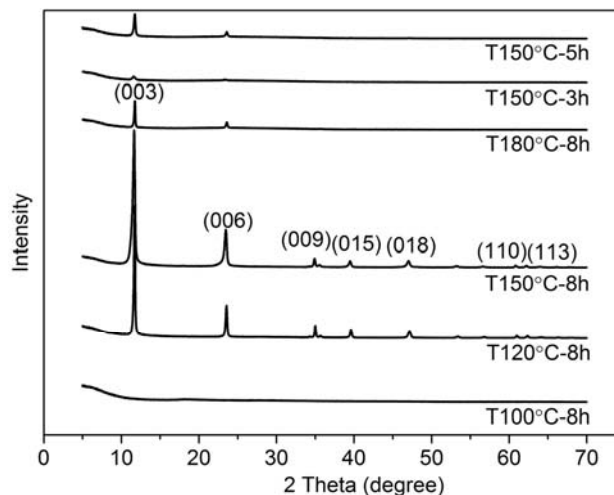
Results and Discussion

Fig. 1 XRD patterns of LDH samples prepared at different bath temperature of 100 ºC-8 h, 120 ºC-8 h, 150 ºC-8 h, 180 ºC-8 h, 150 ºC-3 h and 150 ºC-5 h.

We first characterized the LDH samples prepared in water solvent at different temperature where the synthesis duration was set to be 8 h. The XRD patterns were depicted in Fig. 1. With the temperature of 100 ºC, no observable diffraction peak can be observed, indicating the products may appear as amorphous state. As the bath temperature increased to 120 ºC and 150 ºC, typical diffraction peaks at low angles as indexed by (003), (006), (009) and at high angles for (110), (113) in the XRD patterns suggest the lamellate layers were well crystallized. However, if the bath temperature was set too high (180 ºC in our experiments), the crystalline behaviour was considerably weakened. According to the chemical properties of the precursors we used, we can conclude that the major reason that lead to the observed crystalline behaviours is due to the hydrolysis/decomposition of Urea. Since the LDH nucleation process occurred in a water or water/peroxide environment where the temperature variation should be limited at different bath temperature, the detailed composition of the as-obtained LDH products should be approximate[84, 85], leading to typically observed XRD patterns of Mg–Al–CO_3 LDHs as reported previously[35,86]. On the other aspect, at the liquid-gas interface, the boiled species should be over-heated by the bath and the reflux system will recycle the agents. At relatively low temperature, urea hydrolysis plays the dominant role which provides –OH species for the co-precipitation. The increased bath temperature accelerated the hydrolysis kinetics, leading to better crystalline feature. Over-heating of the liquid/gas phase should result in decomposition of both peroxide and urea to generate O_2, –NCO species and the –OH production might be

lowered. Thereby, high bath temperature should not be beneficial to the crystalline behaviour. In addition, the top two XRD patterns, which belong to the duration of 3 h and 5 h at 150 ºC, indicate that the reaction duration is also essential to the LDH crystallization. Consequently, we assigned 150 ºC and 8 h as the optimal condition in our following studies.
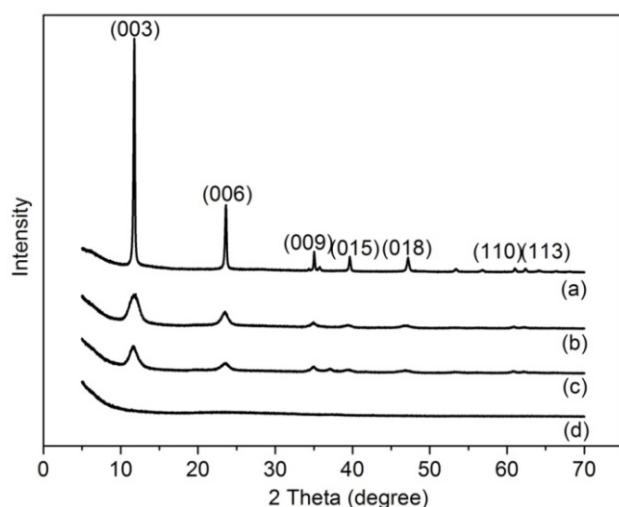

Fig. 2 The XRD patterns of four resultant materials: (a). LDH-W, (b). LDH-P10, (c). LDH-P20 and (d). LDH-P30.
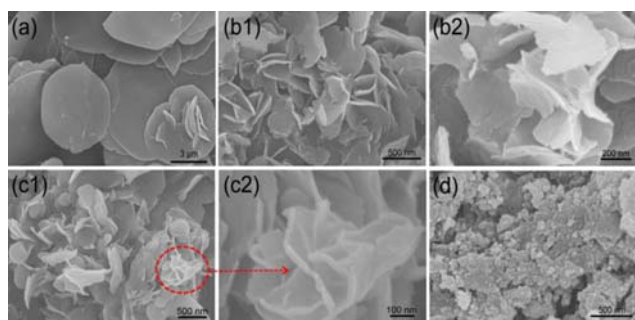

Fig. 3 The SEM image of the samples: (a). LDH-W, (b). LDH-P10, (c). LDH-P20 and (d). LDH-P30.

Similar to the report by Yan et al[83], here we utilized different peroxide/water mixer as solvent (with the peroxide ratio of 10 wt%, 20 wt% and 30 wt%, and the product was denoted by LDH-P10, LDH-P20, LDH-P30, respectively) to carry out the one-pot co-precipitation of Mg-Al-LDH in the same ambient-pressure reflux system. Fig. 2 displays the XRD patterns of the three samples as well as the optimal sample prepared at 150 ºC for 8 h (denoted by LDH-W) for purpose of comparison. Apparently, under the same condition, the introduction of peroxide led to considerable structural changes of LDH. As peroxide concentration increases, the LDH feature peaks gradually diminished and vanished as the H_2O_2 concentration reaches 30 wt%. In general, the weakening of peak (003) and (006) should be an unambiguous clue telling the degree of LDH delamination[76]. In accordance with the SEM characterizations shown in Fig. 3a, uniform and round-shaped LDH sheets can be obtained in water solvent in the ambient-pressure reflux system

with a mean sheet size of 2 µm and a thickness of about 30 nm. The addition of peroxide resulted in a general decrement trend of the LDH size. At 10 wt% (Fig. 3b), the lateral sizes of the LDH-P10 nanosheets were around 0.5 µm, while the thickness of the sheet decreased to about one third of LDH-W, implying that the LDH has been partially delaminated. Once the peroxide concentration was adjusted to 20 wt% (Fig. 3c1), both the particle size and thickness shrank slightly, and the XRD features suggest that the delamination degree was improved. The major difference between these two peroxide concentrations is that, lower peroxide addition led to slight edge bending of the sheets, while higher peroxide addition resulted in severe distortion of the planar sheets. Part of the heavily curved fragments even cross-linked forming the petal-like morphology as shown in Fig. 3c2. As we increased the peroxide ratio to 30 wt% (Fig. 3d), both the vanished XRD peaks and the amorphous SEM morphologies of the sample suggest that the crystalline structure cannot be assembled.
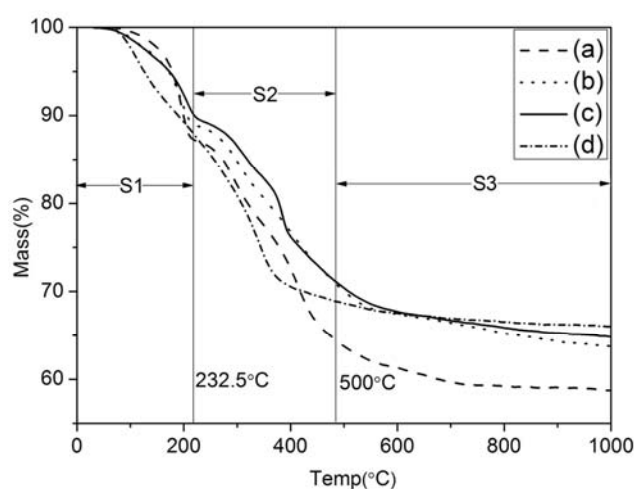

Fig. 4 TG curves of the Mg-Al-CO_3 LDH samples: (a). LDH-W, (b). LDH-P10, (c). LDH-P20 and (d). LDH-P30.

Table 1: The weight loss of two stages for the four samples.

Sample	S1 (30-232.5 ºC)	S2 (232.5-500 ºC)	S3 (500-1000 ºC)
(a). LDH-W	13.08%	23.18%	5.00%
(b). LDH-P10	11.32%	18.68%	6.21%
(c). LDH-P20	10.56%	19.04%	5.58%
(d). LDH-P30	13.17%	18.17%	2.64%

As seen in Fig. 4 and Table 1, for standard Mg-Al-LDH products, there are two distinct weight loss stages within the temperature ranges of 30-232.5 ºC and 232.5-500 ºC, respectively[87, 88]. The first stage (S1) corresponds to the evaporation of the physically adsorbed water molecules around the particle shell and the intercalated water molecules, while the second stage (S2) is ascribed to the thermal decomposition of carbonate groups and the conversion of hydroxide to oxide. As shown in Fig. 4, the weight loss behaviours of the four samples at both the two stages exhibit apparent dependence with respect to the concentration of peroxide. Comparing with LDH-W, both S1 and S2 weight losses decrease when H_2O_2 adding amount is

below 20 wt%, which is led by the shrinking particle sizes and the weakened LDH crystalline feature as elucidated by the XRD and SEM results. Here, we mentioned that for 10 wt% and 20 wt% adding amount of peroxide, the TG curves vary only slightly. While for LDH-P30, the S1 weight loss is the highest due to the strong amorphous morphology and smallest particle sizes which provide more sites for physisorping water molecules. Such a non-crystalline feature implies that the abundance of intercalated carbonate groups is lower than the other three cases, and the S2 weight loss should majorly be attributed to the hydroxide decomposition. Beyond 500℃, the low weight loss of LDH-P30 is the highest due to its noncrystalline nature. For the other three samples, the weight loss of S3 belongs to the final conversion of hydroxides to oxides along with the deconstruction of sheet structures.
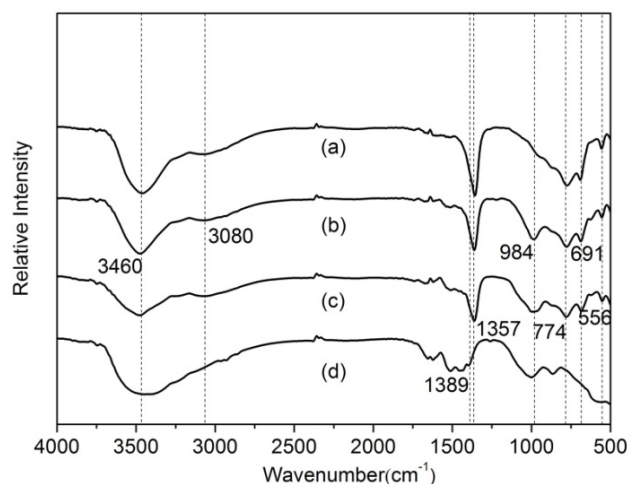

Fig. 5 FT-IR spectra of LDH samples: (a). LDH-W, (b). LDH-P10, (c). LDH-P20 and (d). LDH-P30.

The FT-IR spectra shown in Fig. 5 suggest that the absorption at 3460 cm^{-1}, which belongs to the –OH stretching of the intercalated and absorbed water molecules, were observed for all the four samples. The three peaks at 3080 cm^{-1}, 1357 cm^{-1} and 691 cm^{-1}, associated with the hydrogen bonding of water/carbonate, symmetric stretching and translational mode of carbonate, respectively, had found their presence but except for LDH-P30, which is consistent with our analysis from the TG measurements. Due to the amorphous nature of LDH-P30, the translation modes of hydroxyl ions associated with trivalent aluminium peaked at 774 cm^{-1} and 556 cm^{-1} were also vanished. In addition, the absorption band at around 1389 cm^{-1} can be assigned to the characteristic diffraction peaks of the intercalated nitrate groups which appear only in LDH-P30. Interestingly, a nonnegligible peak at 984 cm^{-1}, which can be assigned to the deformation modes of the –OH groups[89] connecting with Al^{3+}, was observed for all the samples prepared with the addition of peroxide, while was invisible for sample LDH-W assembled in pure water solvent. This motivated us to speculate if the curling or amorphous nature of the LDH-P series can be connected to this unexpected peak and

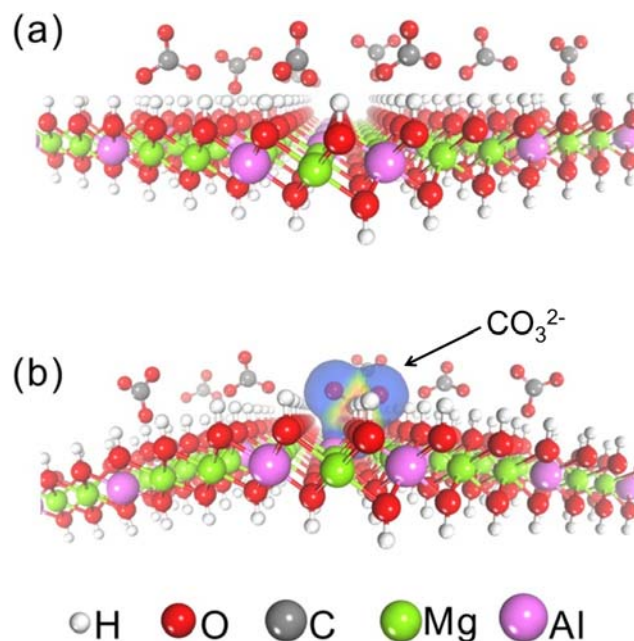consequently to deduce the growing mechanism that governs the assembling of LDH-P samples.

Fig. 6 Schematic illustration of (a) perfect Mg-Al-LDH slab and (b) defective Mg-Al-LDH slab with the defect compensated by carbonate group. The white, red, gray, green and pink atom stands for the H, O, C, Mg and Al atom, respectively.

From the periodic model of the Mg-Al-LDH in Fig. 6a, the –OH groups covering on dual side of the plane all adopt sp^3 hybridization configuration. In a perfect LDH plane, each –OH connects three-foldedly with metal cations and each cation attaches with three hydroxyl groups. At the Al^{3+} sites, extra carbonate groups should be resided nearby to balance the charge. Such a configuration provides strong restriction to the –OH deformation and make each single layer a flat plane. The appearance of the peak at 984 cm^{-1} suggests that the –OH deformation around Al^{3+} has been unlocked for LDH-P10, LDH-P20 and LDH-P30. In accordance with the curved or amorphous morphologies, it implies the existence of point defects in the LDH plane. Considering the fact that, the hydrolysis of urea is the major source of the hydroxyl group, adding peroxide would relatively lower down the –OH production, which would slow down the crystalline process in a certain content. On the other hand, the decomposition of peroxide generates large amounts of oxygen gas, which was supposed to provide the driving force for the delamination[83]. Here, we mentioned that the peroxide decomposition and LDH co-precipitation in fact occur simultaneously, which implies that delamination of large LDH particles might not be realistic.

Instead, we proposed that, when peroxide participates in the reaction, the growth of the LDH-P10, LDH-P20 and LDH-P30 samples should follow a concerted pathway which couples the peroxide decomposition and LDH co-precipitation together. Under such a condition, the generated O_2 would prevent the particles from being ripened. Once a certain amount of nuclei formed, the growth prefer to cumulate at the plane edge but not

to aggregate with adjacent particles. Within this locally gaseous environment, –OH defects have certain probability to appear during co-precipitation and the rest charges are compensated by carbonate groups generated from the urea decomposition. Comparing with perfect Mg-Al-LDH slab (Fig. 6a), the chemically attached carbonate groups at the –OH defects are repulsive to the –OH groups nearby. Such a repulsion will force the planar slab to curve for purpose of releasing the intrinsic stress, as illustrated by Fig. 6b. Due to the chemically-bonding nature, the thermal stability of carbonate groups should be a little bit higher, as evidenced by the higher thermal decomposition temperatures of carbonate in the TG curves in Fig. 4. Simultaneously, the slight blue-shift of the carbonate feature peaks shown in Fig. 5 is also a clear clue for such a compensation form instead of traditional intercalated carbonate. Finally, if the peroxide is excessive, too many O_2 production would remarkably influence the co-precipitation and result in small cross-linked fragments or amorphous state. In fact, those unusual morphologies of LDH products are mostly observed when using urea method as precipitator[65, 80-82]. We believe that the proposed concerted growth mechanism for explaining the curved morphology in our experiments can be also employed to elucidate those atypical growth phenomena.

Conclusions

We implemented a simple one-pot procedure for assembling Mg-Al-CO_3 LDH through co-precipitation method within a reflux system under atmospheric pressure. Using water as a dispersing medium, typical uniform LDH sheets can be obtained at the optimal bath temperature of 150 ºC and duration of 8 h. Under such a condition, as peroxide participated in the process, the morphological features of the as-obtained LDH products are determined by the adding amount of peroxide. Through XRD and SEM characterization, we note that not only the LDH particle sizes decreased with the increasing peroxide concentration, but the products displayed curved or even amorphous nature. The clues in TGA and FT-IR measurements implies that using the set condition, the assembling of Mg-Al-CO_3 LDH may not adopt a typical crystallization-delamination process as reported previously. In fact, we deduced that a locally gaseous environment created by the O_2 from the peroxide decomposition plays an essential role for generating the curved or amorphous morphologies. Besides the function that preventing the particles from being aggregated, –OH point defects occurred and the net charges were compensated by carbonate groups, leading to a defective configuration and presenting as curved sheet or amorphous state.

Acknowledgement

Corresponding Author

* E-mail: cgzhou@cug.edu.cn. wujp@cug.edu.cn.

References

1   Q. Wang and D. O'Hare, *Chem. Rev.*, 2012, **112**, 4124.
2   G. E. David and T. S. Robert C., *Struct. Bond.*, 2006, **119**, 1.
3   K. Aamir I, R. Anusha and F. Bonnie, *Chem. Rev.*, 2009, **48**, 10196.
4   A. I. Khan and D. O'Hare, *J. Mater.*, 2002, **12**, 3191.
5   P. Benito, M. Herrero, F. M. Labajos and V. Rives, *Appl. Clay Sci.*, 2010, **48**, 218.
6   F. Cavani and F. Trifirò, *Catal. Today*, 1991, **11**, 173.
7   J. He, M. Wei, B. Li, Y. Kang, D. G. Evans and X. Duan, *Struct. Bond.*, 2006, **119**, 89.
8   G. R. Williams, A. I. Khan and D. O'Hare, *Struct. Bond.*, 2006, **119**, 161.
9   R. Z. Ma and T. Sasaki, *Adv. Mater.*, 2010, **22**, 5082.
10 S. O'Leary, D. O'Hare and G. Seeley, *Chem. Commun.*, 2002, 1506.
11 L. Qiu, W. Chen, B. Qu, *Polym. Degrad. Stab.*, 2005, **87**, 433.
12 L. Li, R. Ma, Y. Ebina, N. Iyi and T. Sasaki, *Chem. Mater.*, 2005, **17**, 4386.
13 D. P. Yan, J. Lu, M. Wei, J. B. Han, J. Ma, F. Li, D. G. Evans and X. Duan, *Angew. Chem. Int. Edit.*, 2009, **48**, 3073.
14 E. P. Landman and W. W. Focke, S. *Afr. J. Sci.*, 2006, **102**, 581.
15 Y. Z. Bao, L. F. Cong, Z. M. Huang and Z. X. Weng, *J. Mater. Sci.*, 2008, **43**, 390.
16 A. R. Wang, Y. Z. Bao, Z. X. Weng and Z. M. Huang, *Chin. J. Chem. Eng.*, 2008, **16**, 938.
17 D. Sudha and A. Ramasubbu, *Asian J. Chem.* 2013, **25**, S120.
18 F. Leroux and J. P. Besse, *Chem. Mater.*, 2001, **13**, 3507.
19 Q. Z. Yang, D. J. Sun, C. G. Zhang, X. J. Wang and W. A. Zhao, *Langmuir*, 2003, **19**, 5570.
20 M. S. Cho, B. Shin, S. D. Choi, Y. Lee and K. G. Song, *Acta.*, 2004, **50**, 331.
21 J. Tronto, F. Leroux, M. Dubois, J. F. Borin, C. F. Oliveira Graeff and J. B. Valim, *J. Phys. Chem. Solids*, 2008, **69**, 1079.
22 R. Gao, M. J. Zhao, Y. Guan, X. Y. Fang, X. H. Lia and D. P Yan, *J. Mater. Chem. C*, 2014, **2**, 9579.
23 H. Y Ma, R. Gao, D. P. Yan, J. W. Zhao and M. Wei, *J. Mater. Chem. C*, 2013, **1**, 4128.
24 J. M. Oh, S. Y. Kwak, *J. Phys. Chem. Solids.*, 2006, **67**, 1028.
25 M. J. Masarudin, K. Yusoff, R. A. Rahim and M. Z. Hussein, *Nanotechnology*, 2009, **20**, 045602.
26 A. L. McKenzie, C. T. Fishel and R. J. Davis, *J. Catal.* 1992, **138**, 547.
27 B. Sels, D. D. Vos, M. Buntinx, F. Pierard, M. Kirsch-De and P. Jacobs, *Nature*, 1999, **400**, 855.
28 B. Yang and Z. H. Yang, *RSC Adv.* 2013, **3**, 12589.
29 M. Sebastian, C. Nethravathi and M. Rajamathi, *Mater. Res. Bull.*, 2013, **48**, 2715.
30 J. Han, K. C. Roh, M. R. Jo and Y. M. Kang, *Chem. Commun.*, 2013, **49**, 7067.
31 X. M. Fan, Z. H. Yang, R. J. Wen, B. Yang and W. Long, *J. Power Sources*, 2013, **224**, 80.
32 A. B. Béléké, E. Higuchi, H. Inoue and M. Mizuhata, *J. Power Sources*, 2013, **225**, 215.
33 J. W. Zhao, J. Chen, S. Xu, M. F. Shao, D. P. Yan, M. Wei, D. G. Evans and X. Duan, *J. Mater. Chem. A*, 2013, **1**, 8836.
34 D. P. Yan, J. Lu, J. Ma, M. Wei, D. G. Evans and X. Duan, *Angew. Chem. Int. Edit.*, 2011, **50**, 720.
35 D. P. Yan, Y. B. Zhao, M. Wei, R. Z. Liang, J. Lu, D. G. Evans and X. Duan, *RSC Adv.*, 2013, **3**, 4303.
36 A. M. Bashi, S. M. Haddawi and M. A. Arab. Mezaal, *J. Sci. Eng.*, 2013, **38**, 1663.
37 G. Hu, N. Wang, D. O'Hare, J. Davis, *Chem. Commun.*, 2006, 287.
38 G. Hu and D. O'Hare, *J. Am. Chem. Soc.*, 2005, **127**, 17808.
39 G. Hu, N. Wang, D. O'Hare and J. Davis, *J. Mater. Chem.* 2007, **17**, 2257.
40 C. J. Wang, Y. A. Wu, R. M. J. Jacobs, J. H. Warner, G. R. Williams and D. O'Hare, *Chem. Mater.* 2010, **23**, 171.
41 F. Bellezza, A. Cipiciani, U. Costantino, M. Nocchetti and T. Eur. Posati, *J. Inorg. Chem.*, 2009, **2009**, 2603.
42 S. N. Khadzhiev, K. M. Kadiev, G. P. Yampolskaya and M. K. Kadieva, *J. Colloid Interface Sci.*, 2013, **197–198**, 132.

RSC Advances Accepted Manuscript

43 J. Liang, Y. Y. Ma, H. Sun, W. Li and L. X. Wu, *J. Colloid Interface Sci.*, 2013, **409**, 80.

44 J. Stergar, G. Ferk, I. Ban, M. Drofenik, A. Hamler, M. Jagodič and D.Makovec, *J. Alloys Compd.*, 2013, **576**, 220.

45 M. Adachi-Pagano, C. Forano and J. P. Besse, *Chem. Commun.*, 2000, 91.

46 F. Leroux, M. Adachi-Pagano, M. Intissar, S. Chauviere, C. Forano and J. P. Besse, *J. Mater. Chem.*, 2001, **11**, 105.

47 M. Singh, M. I. Ogden, G. M. Parkinson, C. E. Buckley and J. M. Connolly, *J. Mater. Chem.*, 2004, **14**, 871.

48 F. Wypych, G. A. Bubniak, M. Halma and S. Nakagaki, *J. Colloid Interface Sci.*, 2003, **264**, 203.

49 T. Hibino, *Chem. Mater.* 2004, **16**, 5482.

50 Z. P. Liu, R. Z. Ma, M. Osada, N. Iyi, Y. Ebina, K. Takada and T. Sasaki, *J. Amer. Chem. Soc.*, 2006, **128**, 4872.

51 Z. P. Liu, R. Z. Ma, Y. Ebina, N. Iyi, K. Takada and T. Sasaki, *Langmuir,* 2006, **23**, 861.

52 J. B. Liang, R. Z. Ma, N. Iyi, Y. Ebina, K. Takada and T. Sasaki, *Chem. Mater.* 2009, **22**, 371.

53 Y. Zhao, W. D. Yang, Y. H. Xue, X. G. Wang and T. Lin, *J. Mater. Chem.* 2011, **21**, 4869.

54 R. L. Frost, J. Kristof, E. Horvath and J. Kloprogge, *J. Phys. Chem. A,* 1999, **103**, 9654.

55 S. Letaief and C. Detellier, *J. Mater. Chem.,* 2005, **15**, 4734.

56 M. Jobbágy, and A. E. Regazzoni, *J. Colloid Interface Sci.,* 2004, **275**, 345.

57 W. Y. Tseng, J. T. Lin, C. Y. Mou, S. Cheng, S. B. Liu, P. P. Chu and H. W. Liu, *J. Amer. Chem. Soc.,* 1996, **118**, 4411.

58 V. V. Naik, T. N. Ramesh and S. Vasudevan, *J. Phys. Chem. Lett.* 2011, **2**, 1193.

59 J. Gaume, S. Therias, F. Leroux, A. Rivaton and J. L. Gardette, *J. Appl. Polym. Sci.*, 2013, **129**, 1345.

60 X. H. Liu, R. Z. Ma, Y. Bando and T. Sasaki, *Angew. Chem. Int. Ed.,* 2010, **49**, 8253.

61 R. Z. Ma, Z. P. Liu, K. Takada, N. Iyi, Y. Bando and T. Sasaki, *J. Amer. Chem. Soc.,* 2007, **129**, 5257.

62 Q. L. Wu, A. Olafsen, O. B. Vistad, J. Roots and P. Norby, *J. Mater. Chem.* 2005, **15**, 4695.

63 M. Q. Zhao, Q. Zhang, J. Q. Huang and F. Wei, *Adv. Funct. Mater.* 2012, **22**, 675.

64 L. Wang, Z. H. Dong, Z. G. Wang, F. X. Zhang and J. Jin, *Adv. Funct. Mater.* 2013, **23**, 2758.

65 X. H. Liu, R. Z. Ma, Y. Bando and T. A Sasaki, *Adv. Mater.* 2012, **24**, 2148.

66 A. Di Fronzo, C. Pirola, A. Comazzi, F. Galli, C. L. Bianchi, A. Di Michele, R. Vivani, M. Nocchetti, M. Bastianini, D.C. Boffito, Fuel, 2014, 119, 62.

67 J. B. Wei, J. Wang, Y. C. Song, Z. S. Li, Z. Gao, T. Mann and M. L. Zhang, *J. Solid State Chem.*, 2012, **196**, 175.

68 Z. P. Xu, L. Li, C. Y. Cheng, R. G. Ding and C. H. Zhou, *Appl. Clay Sci.,* 2012.

69 Y. Zhou, Y. Kuang, W. Y. Li, Z. L. Chen, M. R. Megharaj and A. Naidu, *Chem. Eng. J.,* 2013, **223**, 68.

70 B. Li and J. He, *J. Phys. Chem. C,* 2008, **112**, 10909.

71 M. Jobbágy and N. Iyi, *J. Phys. Chem. C*, 2010, **114**, 18153.

72 T. Gomez, E. Florez, J. A. Rodriguez and F. Illas, *J. Phys. Chem. C,* 2011, **115**, 11666.

73 F. T. Zhang, L. X. Zhang, D.W. Sun, Y. L. Zhou, Y. L. Ma, Y. R. Qi, L. M. Zhang and X. Xiang, *Sens. Actuators-B: Chem.* 2014, **192**, 150.

74 A. Di Fronzo, C. Pirola, A. Comazzi, F. Galli, C. L. Bianchi, A. Di Michele, R. Vivani, M. Nocchetti, M. Bastianini and D. C. Boffito, *Fuel,* 2014, **119**, 62.

75 S. J. Xia, F. X. Liu, Z. M. Ni, J. L. Xue and P. P. Qian, *J. Colloid Interface Sci.*, 2013, **405**, 195.

76 Q. F. Wang, X. F. Wang, B. Liu, G. Yu, X. J. Hou, D. Chen and G. Z. Shen, *J. Mater. Chem. A*, 2013, **1**, 2468.

77 X. Sun, G. K. Wang, H. T. Sun, F. Y. Lu, M. P. Yu and J. Lian, *J. Power Sources,* 2013, **238**, 150.

78 L. H. Su, Z. W. Song, L. H. Lu and G. L. Pang, *Mater. Res. Bull.* 2013, **8**, 3636.

79 M. Hu, X. D. Ji, L. X. Lei and X. W. Lu, *Electrochim. Acta*, 2013, **105**, 261.

80 M. Adachi-Pagano, C. Forano and J. P. Besse, *J. Mater. Chem.*, 2003, **13**, 1988.

81 J. B. Wei, Z. Gao, Y. C. Song, W. L. Yang, J. Wang, Z. S. Li, T. Mann, M. L. Zhang and L. H. Liu, *Mater. Chem. Phys.*, 2013, **139**, 395.

82 B. Li, J. He, D. G. Evans and X. Duan, *J. Phys. Chem. Solids.*, 2006, **67**, 1067.

83 Y. Yan, Q. Liu, J. Wang, J. Wei, Z. Gao, T. Mann, Z. Li, Y. He, M. Zhang and L. Liu, *J. Colloid Interface Sci.,* 2012, **371**, 15.

84 D. P. Yan, J. Lu, M. Wei, J. Ma, D. G. Evansa and X. Duan. *Phys. Chem. Chem. Phys.,* 2009, **11**, 9200.

85 D. P. Yan, J Lu, M. Wei, J. Ma, D. G. Evansa and X. Duan, *Phys. Chem. Chem. Phys.*, 2010, **12**, 15085.

86 X. B. Wang, Z. M. Bai, D. Zhao, Y. P. Chai, M. Guo and J. Y. Zhang, *Mater. Res. Bull.*, 2013, **48**, 1228.

87 M. Dixit, M. Mishra, P. A. Joshi and D. O. Shah, *J. Ind. Eng. Chem.,* 2013, **19**, 458.

88 X. Y. Xu, D. Q. Li, J. Q. Song, Y. J. Lin, Z. Lv, M. Wei and X. Duan, *Particuology,* 2010, **8**, 198.

89 T. Zhang, Q. R. Li, H. Y. Xiao, H. X. Lu and Y. M. Zhou, *Ind. Eng. Chem. Res.*, 2012, **51**, 11490.